10 mM HEPES, pH 7.4) and incubated with 0.5 mL of the uptake buffer containing quinacrine (1–200 μM) at 37°C for 1–120 min. After incubation, the buffer was removed and cells were washed three times with ice-cold phosphate-buffered saline. The cells were solubilized with 250 μL of 1 N NaOH. Aliquots of the cell solution were removed for protein assay according to the method of Bradford using a Bio-Rad protein assay kit (Bio-Rad Laboratories, Hercules, CA) (Bradford, 1976). Aliquots (200 μL) of the cell solution were neutralized with 200 μL of 1 N HCl and then sample fluorescence was measured (Ex(λ) 450 nm; Em(λ) 530 nm). Quinacrine uptake is expressed as the cell-to-medium ratio (quinacrine amounts in the cells/quinacrine concentration in the medium).

Estimation of Kinetic Parameters

The kinetic parameters for quinacrine uptake by MBEC4 cells were calculated by fitting the uptake rate (V) to the following equation: $V = (V_{max} \times S)/(K_m + S) + P_{dif} \times S$ where V_{max} is the maximum uptake rate of quinacrine (nmol/15 min/mg protein), S is the quinacrine concentration in the medium (μM), K_m is the Michaelis–Menten constant (μM), P_{dif} is the first-order constant for the nonsaturable component (μL/15 min/mg protein). Curve fitting was performed by the nonlinear least-squares regression program, MULTI (Yamaoka *et al.*, 1981).

Detection of OCTN1 mRNA

Total RNA from MBEC4 cells was extracted using TRIZOL™ reagent (Invitrogen, Carlsbad, CA). The primer pair used in the reverse transcription-polymerase chain reaction (RT-PCR) was designed based on the nucleotide sequence of the mouse OCTN1 transporter. The upper primer was 5′-CCTGTTCTGTGTTCCCC-TGT-3′ and the lower primer was 5′-GGTTATGGTGGCAATGTTCC-3′. The expected size of the RT-PCR product, predicted from the positions of the primers, was 232 bp. A SuperScript One-Step RT-PCR system (Invitrogen) was used for reverse transcription of RNA, and OCTN1 cDNA were amplified by PCR. Amplification was performed in a DNA thermal cycler (PC707; ASTEC, Fukuoka, Japan) according to the following protocol: cDNA synthesis for 30 min at 50°C, predenaturation for 2 min at 94°C; 40 cycles of denaturation for 30 s at 94°C, primer annealing for 30 s at 57°C, and polymerization for 30 s at 70°C; and final extension for 5 min at 72°C. Each 10 μL of PCR product was analyzed by electrophoresis on a 3% agarose (Sigma) gel with ethidium bromide staining. The gels were photographed under UV light using a DC290 Zoom digital camera (Kodak, Rochester, New York).

Statistical Analysis

The results are expressed as means ± SEM. Statistical analysis was performed using the Student's unpaired t test. The differences between means were considered to be significant when P values were less than 0.05.

RESULTS

The MBEC4 permeability coefficient of quinacrine dose-dependently increased from $0.58 \pm 0.025 \times 10^{-3}$ to $2.1 \pm 0.15 \times 10^{-3}$ cm/min, when the quinacrine concentration was increased from 50 to 200 μM. The MBEC4 permeability coefficient of quinacrine (100 μM) was significantly lower than that of Na-F (Fig. 1(A)). Permeability coefficients of the basolateral-to-apical transport of quinacrine and Na-F were $1.1 \pm 0.054 \times 10^{-3}$ and $1.5 \pm 0.17 \times 10^{-3}$ cm/min, respectively, while those of the apical-to-basolateral transport were $0.66 \pm 0.023 \times 10^{-3}$ and $1.5 \pm 0.25 \times 10^{-3}$ cm/min, respectively. The basolateral-to-apical transport of quinacrine was significantly higher than that in the opposite direction of transport (Fig. 1(B)). Cyclosporine (10 μM) and verapamil (20 μM) significantly increased the permeability coefficients of the apical-to-basolateral transport of quinacrine from $0.66 \pm 0.023 \times 10^{-3}$ to $1.15 \pm 0.056 \times 10^{-3}$ cm/min and from $0.57 \pm 0.034 \times 10^{-3}$ to $1.02 \pm 0.080 \times 10^{-3}$ cm/min, respectively (Fig. 1(C)).

Quinacrine uptake by MBEC4 cells was time-dependent and reached to the peak at 30 min after the exposure. The cell-to-medium ratio of quinacrine uptake was $2.37 \pm 0.18 \times 10^3$ μL/mg protein at 1 min after the exposure (Fig. 2(A)). Taking the finding that the cell volume of MBEC4 cells is approximately 3 μL/mg protein (Sawada *et al.*, 1999) into consideration, quinacrine is found to be extensively concentrated in MBEC4 cells. To determine whether this apparent concentrative uptake occurs due to only passive entry followed by intracellular binding, MBEC4 cells were treated with 0.015% Triton X for 10 min (Chan *et al.*, 1998). This treatment significantly reduced quinacrine uptake by 30–40% in the period between 30 and 60 min after the addition of quinacrine (Fig. 2(B)). These findings demonstrated that the apparent concentrative accumulation of quinacrine is not due only to passive entry followed by intracellular binding, because quinacrine, when actively accumulated in MBEC4 cells against a concentration gradient and unbound to the binding sites, leaks from cells into the external media through the permeabilized plasma membrane. The initial rate of quinacrine uptake by MBEC4 cells became saturated at 15-min after the exposure to quinacrine (1–200 μM) (Fig. 2(C)). Analysis of these data indicated the involvement of two transport processes (saturable carrier-mediated and nonsaturable system) in quinacrine uptake by MBEC4 cells. The parameters obtained by kinetic analysis were as follows; $V_{max} = 218 \pm 5.4$ nmol/15 min/mg protein, $K_m = 52.1 \pm 1.7$ μM, and passive permeability constant (P_{dif}) $= 94.3 \pm 1.7$ μL/15 min/mg protein.

Quinacrine uptake during a 15-min period was decreased by preincubation of the cells for 10 min with the metabolic inhibitors, NaN_3 (10 mM), DNP (1 mM), and FCCP (10 μM) (Table I). When the experiment was performed at 4°C, quinacrine uptake was reduced (Table I). This uptake was not affected by replacement of the external sodium with N-methylglucamine (Table I) or by changing the external potassium concentration (4.32 ± 0.09, 4.36 ± 0.19, and $4.62 \pm 0.25 \times 10^3$ μL/mg protein at 0, 4.7, and 100 mM of K^+, respectively) (Fig. 3(A)). Pretreatment of MBEC4 cells for a 10-min period with 10 μM of valinomycin, a K^+ ionophore, did not affect quinacrine uptake (Table I). This uptake was elevated from 1.54 ± 0.04 to $4.56 \pm 0.14 \times 10^3$ μL/mg protein by elevating the external pH from 6.4 to 8.4

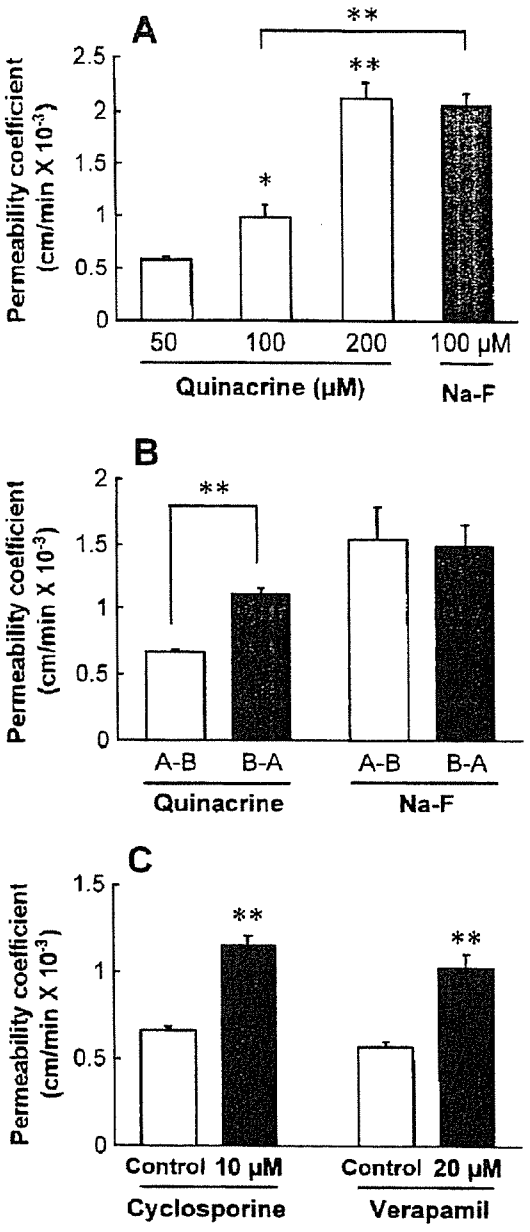

Fig. 1. Characteristics of quinacrine permeability through the MBEC4 monolayer. Panel (A), the permeability coefficients of quinacrine (50–200 μM) or Na-F (100 μM) through the MBEC4 monolayer. Panel (B), the permeability coefficients for the apical-to-basolateral ((A)–(B)) and basolateral-to-apical ((B)–(A)) transport of 100 μM quinacrine and 100 μM Na-F across the MBEC4 monolayer. (A)–(B) and (B)–(A) represent the blood-to-brain and brain-to-blood flux, respectively. Panel (C), the effects of 10 μM cyclosporine and 20 μM verapamil on the apical-to-basolateral transport of 100 μM quinacrine through the MBEC4 monolayer. The permeability coefficient of quinacrine was measured in the presence or absence of each drug. Values are means ± SEM. ($n = 3$–4 (A), 8 ((B), (C))). $^{*}P < 0.05$ and $^{**}P < 0.01$; significant difference from the MBEC4 monolayer treated with 50μM quinacrine (A), the opposite direction (B), and the corresponding control (C).

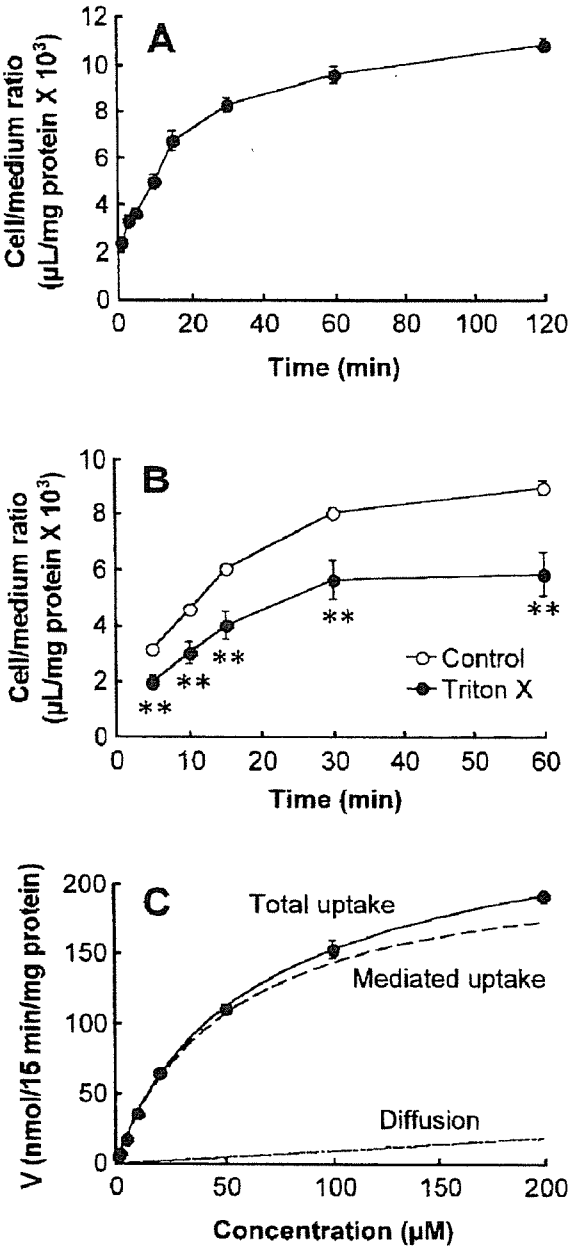

Fig. 2. Characteristics of quinacrine uptake by MBEC4 cells. Panel (A), time course of quinacrine (1 μM) uptake by MBEC4 cells. Panel (B), changes in the quinacrine (1 μM) uptake by MBEC4 cells exposed to 0.015% Triton X for 10 min before the uptake experiment. Panel (C), concentration-dependence of quinacrine uptake by MBEC4 cells. Initial uptake rates at various concentrations of quinacrine (1–200 μM) were measured at 37°C for 15 min. Curves for total, mediated, and diffusive uptake were drawn using the parameters obtained from nonlinear regression analysis (MULTI). Each point represents the mean ± SEM. ($n = 4$–20).** $P < 0.01$; significant difference from the control.

Table I. Effects of Various Compounds and Sodium-Replacement on Uptake of Quinacrine (1 μM) by MBEC4 Cells

Condition	Concentration	Cell/medium ratio (% of control)
NaN_3	10 mM	$67.2 \pm 3.03^{a,**}$
DNP	1 mM	$70.2 \pm 1.79^{a,**}$
4°C		$18.6 \pm 2.22^{a,**}$
FCCP	10 μM	$77.4 \pm 2.49^{a,**}$
Valinomycin	10 μM	97.2 ± 4.22^{a}
Amiloride	1 mM	97.4 ± 3.16^{a}
Tetraethylammonium	1 mM	$88.0 \pm 2.95^{b,**}$
	5 mM	$84.3 \pm 2.93^{b,**}$
	10 mM	$75.4 \pm 4.15^{b,**}$
Cimetidine	1 mM	$81.3 \pm 5.56^{c,**}$
	5 mM	$57.8 \pm 1.70^{c,**}$
	10 mM	$36.8 \pm 1.61^{c,**}$
Na^+ replacement with N-methylglucamine		104 ± 2.87^{d}

[a]MBEC4 cells were preincubated with NaN_3, DNP, FCCP, valinomycin, or amiloride for 10 min. Control values were $4.9 \pm 0.42 \times 10^3$ μL/mg protein. [b,c]Quinacrine uptake was measured by incubating MBEC4 cells with TEA or cimetidine. Control values were 4.1 ± 0.19 and $5.2 \pm 0.19 \times 10^3$ μL/mg protein, respectively.
[d]For investigation of the sodium dependency, quinacrine uptake was measured where Na^+ in the uptake buffer was replaced by N-methylglucamine. Control values were $3.6 \pm 0.22 \times 10^3$ μL/mg protein. Quinacrine uptake was measured at 37°C for 15 min. Values are expressed as % of control. Values are shown as means ± SEM ($n = 4$–20).
$^{**}P < 0.01$; significant difference from the control.

(Fig. 3(B)). These findings demonstrated that quinacrine uptake by MBEC4 cells was pH-dependent. Pretreatment with 10 mM of NaN_3 inhibited quinacrine uptake at each pH used (Table II). Quinacrine uptake was not affected by 1 mM of amiloride (Table I). Therefore, quinacrine uptake was found to be unaffected by Na^+/H^+

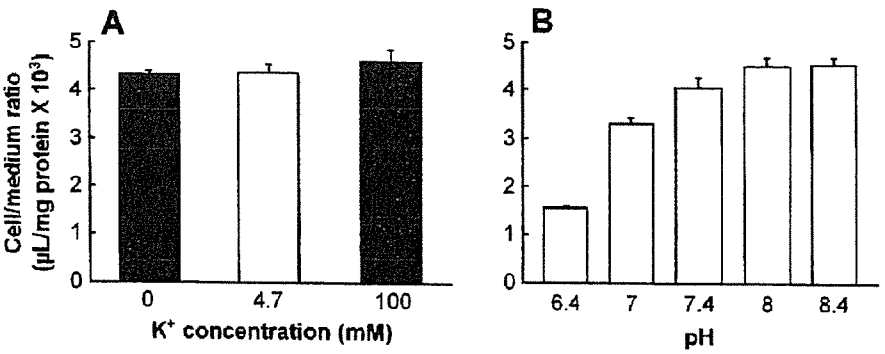

Fig. 3. Effects of the membrane potential (A) and pH (B) on the uptake of quinacrine (1 μM) by MBEC4 cells. Panel (A), effects of various concentrations of external potassium on quinacrine uptake: 0 mM (hyperpolarized), 4.7 mM (control), or 100 mM (depolarized). Panel (B), effects of various pH of the medium on quinacrine uptake. Quinacrine uptake was measured at 37°C for 15 min. Values are expressed as the cell-to-medium ratios. Values are shown as means ± SEM. ($n = 12$).

Table II. Effect of ATP Depletion on the Uptake of Quinacrine (1 μM) by MBEC4 Cells

	Cell/medium ratio (μL/mg protein $\times 10^3$)	
pH	Normal	ATP-depletion
6.4	1.61 ± 0.02	1.36 ± 0.03**
7.0	3.53 ± 0.14	3.28 ± 0.10
7.4	3.95 ± 0.32	3.20 ± 0.33*
8.0	4.71 ± 0.35	3.87 ± 0.30
8.4	4.77 ± 0.19	3.82 ± 0.22*

MBEC4 cells were preincubated with 10 mM NaN_3 for 10 min (ATP depletion). Quinacrine uptake was measured at 37°C for 15 min. Values are shown as means ± SEM ($n = 3$–8).
*$P < 0.05$, **$P < 0.01$; significant difference from the control.

exchange. The effects of organic cations and P-gp inhibitors on quinacrine uptake were investigated. The organic cations including TEA (1-10 mM) and cimetidine (1–10 mM) significantly reduced quinacrine uptake by 12–25% and 19–65%, respectively (Table I). In the presence of cyclosporine (10 μM) or verapamil (20 μM), quinacrine uptake under the steady-state significantly increased by about 10% (Fig. 4).

To provide molecular evidence for the expression of OCTN1 in MBEC4 cells, RT-PCR was carried out (Fig. 5). With a primer pair specific for mouse OCTN1, RT-PCR with mRNA obtained from MBEC4 cells yielded a single product. The size of this product was the same as that expected from the primer positions in mouse OCTN1.

DISCUSSION

The BBB permeability coefficient of quinacrine, a candidate for the treatment of CJD, was much lower than that of Na-F, a BBB-impermeable marker, suggesting that

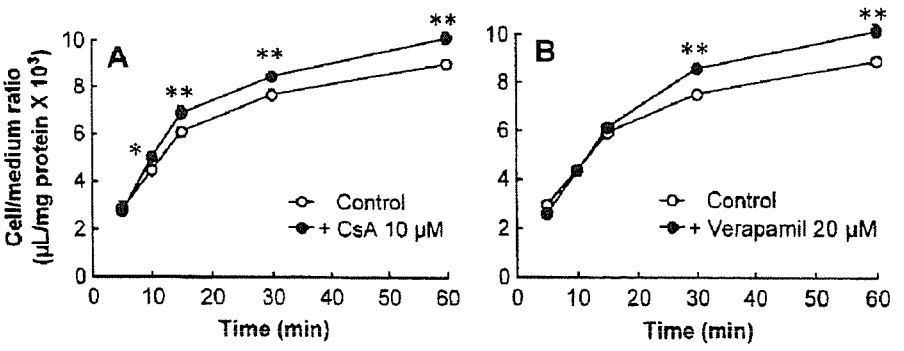

Fig. 4. Effects of 10 μM cyclosporine (A) and 20 μM verapamil (B) on uptake of quinacrine (1 μM) by MBEC4 cells. Quinacrine uptake was measured at 37°C in the absence and presence of cyclosporine or verapamil. Values are expressed as the cell-to-medium ratios. Values are shown as means ± SEM. ($n = 8$).

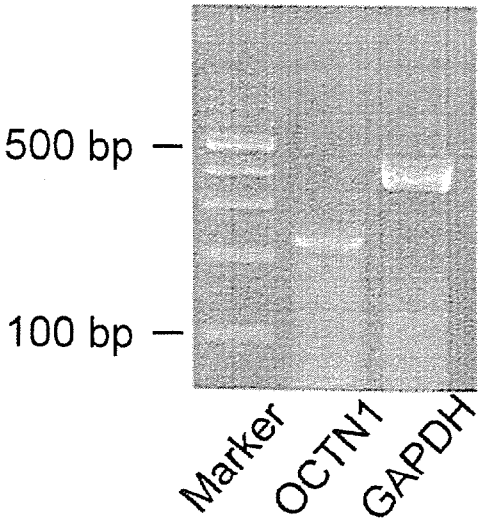

Fig. 5. Photograph showing OCTN1 expression in MBEC4 cells by RT-PCR. RNA samples from MBEC4 cells were used for RT-PCR with primer pairs specific for mouse OCTN1.

the permeability of quinacrine into the brain through the BBB is extremely low. To determine which machinery is involved in the low permeability of quinacrine across the BBB, we investigated the polarity of transcellular transport of quinacrine and the effects of P-gp inhibitors (cyclosporine and verapamil) on the BBB permeability of quinacrine. The basolateral-to-apical (brain-to-blood) transport of quinacrine across MBEC4 monolayer was greater than quinacrine transport in the opposite direction (Fig. 1(B)). Cyclosporine and verapamil increased the apical-to-basolateral (blood-to-brain) transport of quinacrine (Fig. 1(C)). Quinacrine uptake by MBEC4 cells under the steady-state was significantly increased by cyclosporine and verapamil (Fig. 4). These findings indicate the possible involvement of P-gp in the efflux transport of quinacrine. P-gp largely contributes to multidrug-resistance of the BBB in an ATP-dependent manner. This study provided controversial evidence that metabolic inhibitors or incubation at low temperature decreased quinacrine uptake (Table I). Quinacrine was actively and concentratively accumulated in MBEC4 cells. A large part of quinacrine is probably taken up via the saturable system, although quinacrine uptake was shown to have both saturable and nonsaturable pathways (Fig. 2(C)). Uptake of quinacrine by choroid plexus cells was organic cation-specific and energy-dependent (Miller *et al.*, 1999). In light of these findings, P-gp (an efflux system) and other influx transport system(s) are considered to mediate quinacrine transport into the brain.

We elucidated a role of the known organic cation transporters (OCT1, OCT2, OCT3, OCTN1, and OCTN2), and the specificity or driving force of those transporters in mediating quinacrine uptake by MBEC4 cells. Quinacrine uptake was significantly inhibited by various organic cations including TEA and cimetidine, which are known to be a substrate and an inhibitor of the organic cation transporters, respectively. Quinacrine uptake was insensitive to changes in the membrane potential (Fig. 3(A)) and strongly inhibited by lowering the external pH (Fig. 3(B)). These characteristics are distinct from those of the OCT1, OCT2, and OCT3, all of which

are dependent on the membrane potential (Gorboulev *et al.*, 1997; Grundemann *et al.*, 1994; Kekuda *et al.*, 1998). Considering quinacrine is an organic base, the pH-related decrease in quinacrine uptake may have resulted from an increase in the concentration of ionized quinacrine according to the pH partition theory. However, our data showing that quinacrine uptake by MBEC4 cells at each pH was inhibited by NaN_3 (Table II) suggest that a pH-sensitive transport system is involved in quinacrine uptake. Transport of quinacrine increased by elevating the outward H^+ gradient across the membrane. This finding indicates that quinacrine may be transported through MBEC4 cells by an H^+/quinacrine antiport. The activity of H^+/organic cation antiporter is regulated by pH or H^+ gradient as the driving force (Maegawa *et al.*, 1988). The H^+ gradient is formed by Na^+/H^+ exchange in the vicinity of the apical membrane of brain endothelial cells (Ennis *et al.*, 1996). The Na^+/H^+ exchange is, however, unlikely to participate in quinacrine uptake by MBEC4 cells, since Na^+-depletion and amiloride failed to reduce quinacrine uptake (Table I). OCTN1 is Na^+-independent organic cation transporter (Wu *et al.*, 2000). OCTN2 mediates uptake of L-carnitine and several organic cations in an Na^+-coupled and Na^+-independent manner, respectively (Wu *et al.*, 1999). OCTN1 is a pH-dependent organic cation transporter presumably energized by a proton antiport mechanism (Yabuuchi *et al.*, 1999). The characteristics of quinacrine transport obtained in this study are similar to those of OCTN1. Mouse OCTN1 is distributed in the brain, heart, and liver, and strongly expressed in the kidney (Tamai *et al.*, 2000). RT-PCR analysis of MBEC4 cells demonstrated the expression of OCTN1 (Fig. 5). Therefore, OCTN1 is suggested to be a potential transporter mediating quinacrine uptake by MBEC4 cells.

The BBB permeability of quinacrine was extremely low, although quinacrine was rapidly transported into the brain endothelial cells by the apical pH-dependent transport system. A weak organic base binds to a variety of polyanions including RNA, DNA, and ATP, and accumulates in the acidic intracellular compartments (Miller *et al.*, 1999). Quinacrine is distributed in the nucleus and vesicular compartment in the cytoplasm of choroid plexus cells (Miller *et al.*, 1999). In the brain endothelial cells, a large part of quinacrine was shown to be distributed and accumulated in the intracellular binding compartment (Fig. 2(B)). The resulting small part of quinacrine in the intracellular nonbinding compartment appears to contribute to the BBB permeability. The P-gp-mediated active efflux at the apical side of the plasma membrane and the large storage capacity in the cytoplasm are considered to restrict the entry of quinacrine into the brain. The mechanism involved in quinacrine transport at the basolateral side remains obscure.

In conclusion, quinacrine transport at the BBB is mediated by the influx and efflux transport systems. The influx of quinacrine is mediated by a pH-dependent and Na^+- and membrane potential-independent system, an OCTN1-like transporter. The efflux of quinacrine evoked by P-gp at the BBB restricts the entry of quinacrine into the brain. This phenomenon may be interpreted as lowering the therapeutic efficacy of quinacrine for CJD. This study may have clinical implications; quinacrine concentrations in the brain increased by P-gp modulators including verapamil may enhance the therapeutic efficacy of quinacrine for CJD.

ACKNOWLEDGMENTS

This work was supported in part by a Grant-in-Aid for Scientific Research ((B)(2) 14370789) from the Ministry of Education, Culture, Sports, Science, and Technology (MEXT), Japan.

REFERENCES

Bradford, M. M. (1976). A rapid and sensitive method for the quantitation of microgram quantities of protein utilizing the principle of protein dye binding. *Anal. Biochem.* **72:**248–254.

Chan, B. S., Satriano, J. A., Pucci, M., and Schuster, V. L. (1998). Mechanism of prostaglandin E_2 transport across the plasma membrane of HeLa cells and Xenopus oocytes expressing the prostaglandin transporter "PGT". *J. Biol. Chem.* **273:**6689–6697.

Dehouck, M.-P., Jolliet-Riant, P., Brée, F., Fruchart, J.-C., Cecchelli, R., and Tillement, J.-P. (1992). Drug transfer across the blood–brain barrier: Correlation between in vitro and in vivo models. *J. Neurochem.* **58:**1790–1797.

Ennis, S. R., Ren, X., and Betz, A. L. (1996). Mechanisms of sodium transport at the blood-brain barrier studied with in situ perfusion of rat brain *J. Neruochem.* **66:**756–763.

Follette, P. (2003). Prion disease treatment's early promise unravels. *Science* **299:**191–192.

Friedrich, A., George, R. L., Bridges, C. C., Prasad, P. D., and Ganapathy, V. (2001). Transport of cholin and its relationship to the expression of organic cation transporters in a rat brain microvessel cell line (RBE4). *Biochim. Biophys. Acta* **1512:**299–307.

Friedrich, A., Prasad, P. D., Freyer, D., Ganapathy, V., and Brust, P. (2003). Molecular cloning and functional characterization of the OCTN2 transporter at the RBE4 cells, an in vitro model of the blood-brain barrier. *Brain Res.* **968:**69–79.

Gorboulev, V., Ulzheimer, J. C., Akhoundova, A., Ulzheimer-Teuber, I., Karbach, U., Quester, S., Baumann, C., Lang, F., Busch, A. E., and Koepsell, H. (1997). Cloning and characterization of two human polyspecific organic cation transporters. *DNA Cell Biol.* **16:**871–881.

Grundemann, D., Gorboulev, V., Gambaryan, M., Vehyhl, M., and Koepsell, H. (1994). Drug excretion mediated by a new prototype of polyspecific transporter. *Nature* **372:**549–552.

Kekuda, R., Prasad, P. D., Wu, X., Wang, H., Fei, Y. J., Leibach, F. H., and Ganapathy, V. (1998). Cloning and functional characterization of a potential-sensitive, polyspecific organic cation transporter (OCT3) most abundantly expressed in placenta. *J. Biol. Chem.* **273:**15971–15979.

Koepsell, H. (1998). Organic cation transporters in intestine, kidney, liver, and brain. *Annu. Rev. Physiol.* **60:**243–266.

Korth, C., May, B. C. H., Cohen, F. E., and Prusiner, S. B. (2001). Acridine and phenothiazine derivatives as pharmacotherapeutics for prion disease. *Proc. Natl. Acad. Sci. U.S.A.* **98:**9836–9841.

Maegawa, H., Kato, M., Inui, K., and Hori, R. (1988). pH sensitivity of H^+/organic cation antiport system in rat renal brush-border membranes. *J. Biol. Chem.* **263:**11150–11154.

Miller, D. S., Villalobos, A. R., and Pritchard, J. B. (1999). Organic cation transport in rat choroid plexus cells studied by fluorescence microscopy. *Am. J. Physiol.* **276:**C955–C968.

Okuda, N., Saito, H., Urakami, Y., Takano, M., and Inui, K. I. (1996). cDNA cloning and functional expression of a novel rat kidney organic cation transporter. *Biochem. Biophys. Res. Commun.* **224:**500–507.

Sawada, N., Takanaga, H., Matsuo, H., Naito, M., Tsuruo, T., and Sawada, Y. (1999). Choline uptake by mouse brain capillary endothelial cells in culture. *J. Pharm. Pharmacol.* **51:**847–852.

Sweet, D. H., and Pritchard, J. (1999). rOCT2 is a basolateral potential-driven carrier, not an organic cation/proton exchanger. *Am. J. Physiol.* **277:**F890–F898.

Tamai, I., Ohashi, R., Nezu, J., Sai, Y., Kobayashi, D., Oku, A., Shimane, M., and Tsuji, A. (2000). Molecular and functional characterization of organic cation/carnitine transporter family in mice. *J. Biol. Chem.* **275:**40064–40072.

Tamai, I., Yabuuchi, H., Nezu, J., Sai, Y., Oku, A., Shimane, M., and Tsuji, A. (1997). Cloning and characterization of a novel human pH-dependent organic cation transporter, OCTN1. *FEBS Lett.* **419:**107–111.

Tatsuta, T., Naito, M., Mikami, K., and Tsuruo, T. (1994). Enhanced expression by the brain matrix of P-glycoprotein in brain capillary endothelial cells. *Cell Growth Differ.* **5:**1145–1152.

Tatsuta, T., Naito, M., Oh-hara, T., Sugawara, I., and Tsuruo, T. (1992). Functional involvement of P-glycoprotein in blood–brain barrier. *J. Biol. Chem.* **267:**20383–20391.

Wu, X., George, R. L., Huang, W., Wang, H., Conway, S. J., Leibach, F. H., and Ganapathy, V. (2000). Structural and functional characteristics and tissue distribution pattern of rat OCTN1, an organic cation transporter, cloned from placenta. *Biochim. Biophys. Acta* **1466**:315–327.

Wu, X., Huang, W., Prasad, P. D., Seth, P., Rajan, D. P., Leibach, F. H., Chen, J., Conway, S. J., and Ganapathy, V. (1999). Functional characteristics and tissue distribution pattern of organic cation transporter 2 (OCTN2), an organic cation/carnitine transporter. *J. Pharmacol. Exp. Ther.* **290**:1482–1492.

Wu, X., Prasad, P. D., Leibach, F. H., and Ganapathy, V. (1998). cDNA sequence, transport function, and genomic organization of human OCTN2, a new member of the organic cation transporter family. *Biochem. Biophys. Res. Commun.* **246**:589–595.

Yabuuchi, H., Tamai, I., Nezu, J., Sakamoto, K., Oku, A., Shimane, M., Sai, Y., and Tsuji, A. (1999). Novel membrane transporter OCTN1 mediates multispecific, bidirectional, and pH-dependent transport of organic cations. *J. Pharmacol. Exp. Ther.* **289**:768–773.

Yamaoka, K., Tanigawara, Y., Nakagawa, T., and Uno, T. (1981). A pharmacokinetic analysis program (MULTI) for microcomputer. *J. Pharmacobiodyn.* **4**:879–885.

Cellular and Molecular Neurobiology, Vol. 24, No. 3, June 2004 (© 2004)

Rapid Communication

Transforming Growth Factor-β1 Upregulates the Tight Junction and P-glycoprotein of Brain Microvascular Endothelial Cells

Shinya Dohgu,[1,2] Atsushi Yamauchi,[2] Fuyuko Takata,[2] Mikihiko Naito,[3] Takashi Tsuruo,[3] Shun Higuchi,[1] Yasufumi Sawada,[1] and Yasufumi Kataoka[2,4]

Received September 29, 2003; accepted October 10, 2003

SUMMARY

1. The present study was aimed at elucidating effects of transforming growth factor-β (TGF-β) on blood–brain barrier (BBB) functions with mouse brain capillary endothelial (MBEC4) cells.

2. The permeability coefficients of sodium fluorescein and Evans blue albumin for MBEC4 cells and the cellular accumulation of rhodamine 123 in MBEC4 cells were dose-dependently decreased after a 12-h exposure to TGF-β1 (0.01–10 ng/mL).

3. The present study demonstrates that TGF-β lowers the endothelial permeability and enhances the functional activity of P-gp, suggesting that cellular constituents producing TGF-β in the brain may keep the BBB functioning.

KEY WORDS: transforming growth factor-β; blood–brain barrier; permeability; P-glycoprotein; mouse brain endothelial cells.

INTRODUCTION

The Blood–brain barrier (BBB) is highly restrictive of the transport of substances between blood and the central nervous system. The BBB is a complex system of different cellular component consisting brain microvascular endothelial cells, pericytes

[1] Department of Medico-Pharmaceutical Sciences, Graduate School of Pharmaceutical Sciences, Kyushu University, Higashi-ku, Fukuoka, Japan.

[2] Department of Pharmaceutical Care and Health Sciences, Faculty of Pharmaceutical Sciences, Fukuoka University, Jonan-ku, Fukuoka, Japan.

[3] Institute of Molecular and Cellular Biosciences, University of Tokyo, Bunkyo-ku, Tokyo, Japan.

[4] To whom correspondence should be addressed at Department of Pharmaceutical Care and Health Sciences, Faculty of Pharmaceutical Sciences, Fukuoka University, 8-19-1 Nanakuma, Jonan-ku, Fukuoka 814-0180, Japan; e-mail: ykataoka@cis.fukuoka-u.ac.jp.

0272-4340/04/0600-0491/0

and astrocytes. Astrocytes induce and maintain the properties of the BBB including the integration of tight junctions and expression of P-glycoprotein (P-gp) through cell-to-cell contact and secretion of soluble factors (Rubin and Staddon, 1999). Brain pericytes are important for the control of growth and migration of endothelial cells and the integrity of microvascular capillaries (Ramsauer *et al.*, 2002). These functions are mediated, at least in part, by transforming growth factor-β (TGF-β), a family of multifunctional peptide growth factors (Orlidge and D'Amore, 1987; Sato and Rifkin, 1989). TGF-β isoforms (TGF-β1, 2, 3, 4, and 5) share the same structure (65–80% homology) and display similar biological activity in vitro (Flanders *et al.*, 1998). TGF-β is listed as a compound protecting against neurodegeneration (Flanders *et al.*, 1998). Several cytokines and growth factors influence on the permeability of the BBB, such as vascular endothelial growth factor (Wang *et al.*, 1996) and tumor necrosis factor-α (Deli *et al.*, 1995). However, little is known about the role of TGF-β in the maintenance of BBB function. In the present study, effects of TGF-β1 were examined on the permeability of brain endothelial cells and the functional activity of P-gp. We used mouse brain endothelial (MBEC4) cells showing the highly specialized characteristics of brain microvascular endothelial cells including the expression of P-gp (Tatsuta *et al.*, 1992, 1994).

MATERIALS AND METHODS

MBEC4 cells, which were isolated from BALB/c mouse brain cortices and immortalized by SV40-transformation (Tatsuta *et al.*, 1992), were cultured in Dulbecco's modified Eagle's medium (DMEM) (GIBCO BRL, Life Technologies, Grand Island, NY) supplemented with 10% fetal bovine serum, 100 units/mL of penicillin, and 100 μg/mL of streptomycin. They were grown in 12-well Transwells^{TM} (Costar, MA) and 24-well plates (FALCON; Becton Dickinson Labware, Lincolin Park, NJ) in a humidified atmosphere of 5% CO_2/95% air at 37°C.

MBEC4 cells (42,000 cells/cm^2) were cultured on the collagen-coated polycarbonate membrane (3.0 μm pore size) of the Transwell^{TM} insert (12-well type). After culture for 3 days, they were washed three times with serum-free medium. Cells were exposed to 0.01–10 ng/mL of TGF-β1 (Sigma, St. Louis) injected into the inside of the insert (luminal side) for 12 h. To initiate the transport experiments, the medium was removed and cells were washed three times with Krebs–Ringer buffer (118 mM NaCl, 4.7 mM KCl, 1.3 mM $CaCl_2$, 1.2 mM $MgCl_2$, 1.0 mM NaH_2PO_4, 25 mM $NaHCO_3$, and 11 mM D-glucose, pH 7.4). Krebs–Ringer buffer (1.5 mL) was added outside of the insert (abluminal side). Krebs–Ringer buffer (0.5 mL) containing 100 μg/mL of sodium fluorescein (Na-F) (MW 376, Sigma, St. Louis) and 4% bovine serum albumin (Sigma, St. Louis) mixed with 0.67 mg/mL of Evans blue dye (EBA) (MW 67,000, Wako, Osaka, Japan) was loaded on the luminal side of the insert. Samples (0.5 mL) were removed from the abluminal chamber at 10, 20, 30, and 60 min and immediately replaced with fresh Krebs–Ringer buffer. Aliquots (5 μL) from the abluminal chamber samples were mixed with 200 μL of Krebs–Ringer buffer and then the concentration of Na-F was determined using a multiwell fluorometer (Ex(λ) 485 nm; Em(λ) 530 nm) (CytoFluor Series 4000, PerSeptive Biosystems, Framingham, MA).

The EBA concentration in the abluminal chamber was measured by determining the absorbance of aliquots (150 μL) at 630 nm with a microplate reader (Opsys MR, DYNEX technologies, Chantilly, VA). The permeability coefficient and clearance were calculated according to the method described by Dehouck *et al.* (1992). Clearance was expressed as microliter (μL) of tracer diffusing from the luminal to abluminal chamber and was calculated from the initial concentration of tracer in the luminal and final concentration in the abluminal chamber: Clearance (μL) = $[C]_A \times V_A/[C]_L$ where $[C]_L$ is the initial luminal tracer concentration, $[C]_A$ is the abluminal tracer concentration, and V_A is the volume of the abluminal chamber. During a 60-min period of the experiment, the clearance volume increased linearly with time. The average volume cleared was plotted versus time, and the slope was estimated by linear regression analysis. The slope of clearance curves for the MBEC4 monolayer was denoted PS_{app}, where PS is the permeability $\times$ surface area product (in μL/min). The slope of the clearance curve with a control membrane was denoted $PS_{membrane}$. The real PS value for the MBEC4 monolayer (PS_{trans}) was calculated from $1/PS_{app} = 1/PS_{membrane} + 1/PS_{trans}$. The PS_{trans} values were divided by the surface area of the Transwell inserts to generate the permeability coefficient (P_{trans}, in cm/min).

The functional activity of P-gp was determined by measuring the cellular accumulation of rhodamine 123 (Sigma, St. Louis) according to the method of Fontaine *et al.* (1996). MBEC4 cells (21,000 cells/cm^2) were cultured on the collagen-coated 24-well plates. Three days after seeding cells, they were washed three times with serum-free medium and then exposed to 0.01–10 ng/mL of TGF-β1 for 12 h. The medium was removed and cells were washed three times with assay buffer (143 mM NaCl, 4.7 mM KCl, 1.3 mM $CaCl_2$, 1.2 mM $MgCl_2$, 1.0 mM NaH_2PO_4, 10 mM HEPES, and 11 mM D-glucose, pH 7.4). Cells were incubated with 0.5 mL of assay buffer containing 5 μM rhodamine 123 for 1 h. Then, the solution was removed and cells were washed three times with ice-cold phosphate-buffered saline and solubilized in 0.2 N NaOH (0.5 mL). The rhodamine 123 content was determined using a multiwell fluorometer (Ex(λ) 485 nm; Em(λ) 530 nm) (CytoFluor Series 4000, PerSeptive Biosystems, Framingham, MA). The cellular protein was measured by the method of Bradford (1976).

The values are expressed as means $\pm$ SEM. Statistical analysis was performed using Student's unpaired t test. A single-factor analysis of variance (ANOVA) followed by the Dunnett test was applied to multiple comparisons. The differences between means were considered to be significant when P values were less than 0.05.

RESULTS

TGF-β1 at a concentration of 10 ng/mL significantly decreased the permeability of the cells to Na-F and EBA at 3 h by 71.9 and 55.5% of control, respectively, during a period of 6–12 h (Fig. 1(A) and (B)). The permeability coefficients of Na-F and EBA for MBEC4 cells were dose-dependently reduced by 1.7–38.8% and 8.4–42.1%, respectively, after a 12-h exposure to TGF-β1 (0.01–10 ng/mL) (Fig. 1(A) and (B)). As shown in Fig. 2, the cellular accumulation of rhodamine 123 into MBEC4 cells was dose-dependently reduced by 69.0–100.7%

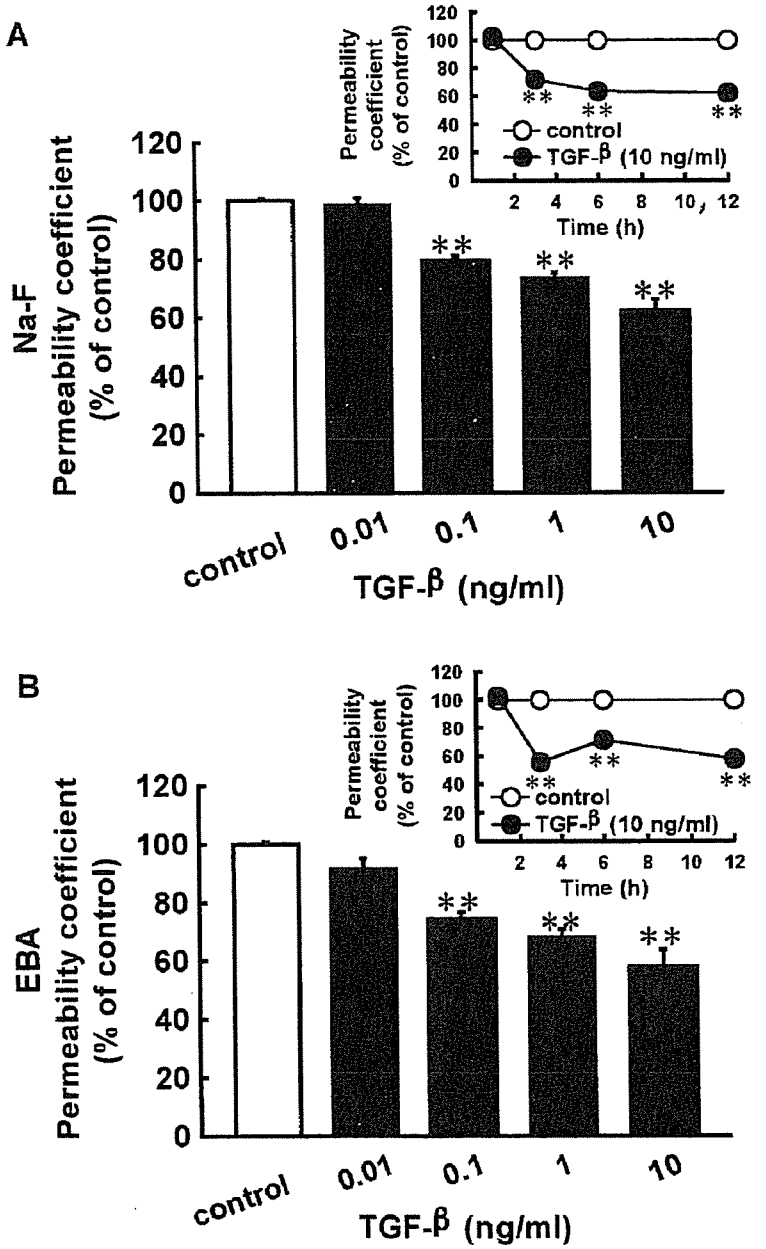

Fig. 1. Changes in the permeability coefficient of Na-F (A) and EBA (B) in MBEC4 cell monolayers after exposure to various concentrations of TGF-β1 for 12 h. The permeability coefficients of Na-F and EBA for the control in panel A and B were 2.71 ± 0.09 × 10^{-4} and 0.85 ± 0.05 × 10^{-4} cm/min, respectively. The inset in each panel shows the time-course of the permeability coefficient of Na-F and EBA after exposure to 10 ng/mL of TGF-β1. The permeability coefficients of Na-F and EBA for the control were 1.34 ± 0.02, 2.10 ± 0.05, 2.17 ± 0.01, and 3.01 ± 0.13 × 10^{-4} cm/min in the inset of panel A (Na-F) for 1, 3, 6, and 12 h, respectively, and 0.46 ± 0.02, 0.97 ± 0.02, 0.66 ± 0.03, and 1.02 ± 0.08 × 10^{-4} cm/min in the inset of panel B (EBA) for 1, 3, 6, and 12 h, respectively. Data are expressed as percentages of control. Values are shown as means ± SEM (n = 4–24). $^{**}P < 0.01$; significant difference from control.

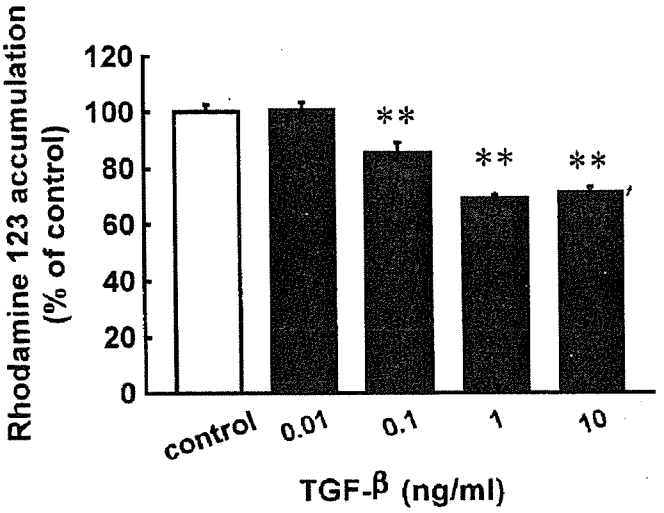

Fig. 2. Changes in the cellular accmulation of rhodamine 123 in MBEC4 cells after exposure to various concentrations of TGF-β1 for 12 h. The cellular accumulation of rhodamine 123 in MBEC4 cells for the control was 1.65 ± 0.05 nmol/mg protein. Data are expressed as percentages of control. Values are shown as means ± SEM ($n = 4$–10). $^{**}P < 0.01$; significant difference from control.

of control after a 12-h exposure to TGF-β1 at concentrations ranging from 0.1 to 10 ng/mL.

DISCUSSION

The permeability of Na-F and EBA through the MBEC4 monolayer was reduced by TGF-β1 and the accumulation of rhodamine 123 into MBEC4 cells was significantly decreased by TGF-β1. This action of TGF-β1 appeared within 3 h after treatment. These findings suggest that TGF-β1 supports the maintenance of BBB functions by integrating tight junctions and activating a P-gp-related transport system. The epithelial and endothelial barrier of paracellular permeability through tight junctions is known to be regulated by various signaling molecules including protein kinase C. Activation of protein kinase C is involved in the TGF-β signaling pathway (Halstead *et al.*, 1995), leading to a decrease in the permeability of brain microvascular endothelial cells (Raub, 1996). TGF-β-enhanced BBB functions in the early stage may be interpreted as occurring due to protein kinase C activation. TGF-β mediates multifunctional effects by eliciting transcriptional responses in many target genes. TGF-β1 increased *mdr1* gene expression via a protein kinase C-related signal transduction pathway (Utsunomiya *et al.*, 1997). The other TGF-β signaling cascades from membrane to nucleus could be involved in an enhancement of BBB functions, such as mitogen-activated protein kinase (Hartsough and Mulder, 1995) and a receptor serine/threonine kinase pathway (Wrana *et al.*, 1994). It is, therefore,

conceivable that TGF-β facilitates the barrier function and P-gp functional activity of brain endothelial cells by increasing the expression of tight junction-associated proteins (such as occludin and claudins) and P-gp. Endothelial cells, when co-cultured with pericytes, produced an activated form of TGF-β (Antonelli-Olridge *et al.*, 1989) and elevated transendothelial electrical resistance (Dente *et al.*, 2001), suggesting that TGF-β production by pericytes is significant for maintaining the integrity of the BBB.

In the present study, we demonstrated that TGF-β1 lowered endothelial permeability and increased the functional activity of the P-gp efflux pump in MBEC4 cells. These findings suggest that cellular constituents producing TGF-β in the brain may keep the BBB functioning.

ACKNOWLEDGMENTS

This work was supported in part by a Grant-in-Aid for Scientific Research ((B)(2) 14370789) from the Ministry of Education, Culture, Sports, Science and Technology (MEXT), Japan, and by funds (No. 031001) from the Central Research Institute of Fukuoka University.

REFERENCES

Antonelli-Orlidge, A., Saunders, K. B., Smith, S. R., and D'Amore, P. A. (1989). An activated form of transforming growth factor β is produced by cocultures of endothelial cells and pericytes. *Proc. Natl. Acad. Sci. U.S.A.* **88:**4544–4548.

Bradford, M. M. (1976). A rapid and sensitive method for the quantitation of microgram quantities of protein utilizing the principle of protein-dye binding. *Anal. Biochem.* **72:**248–254.

Dehouck, M.-P., Jolliet-Riant, P., Brée, F., Fruchart, J.-C., Cecchelli, R., and Tillement, J.-P. (1992). Drug transfer across the blood–brain barrier: Correlation between in vitro and in vivo models. *J. Neurochem.* **58:**1790–1797.

Deli, M. A., Descamps, L., Dehouck, M.-P., Cecchelli, R., Joó, F., Ábrahám, C. S., and Torpier, G. (1995). Exposure of tumor necrosis factor-α to luminal membrane of bovine brain capillary endothelial cells cocultured with astrocytes induces a delayed increase of permeability and cytoplasmic stress fiber formation of actin. *J. Neurosci. Res.* **41:**717–726.

Dente, C. J., Steffes, C. P., Speyer, C., and Tyburski, J. G. (2001). Pericytes augment the capillary barrier in in vitro cocultures. *J. Surg. Res.* **97:**85–91.

Flanders, K. C., Ren, R. F., and Lippa, C. P. (1998). Transforming growth factor-βs in neurodegenerative disease. *Prog. Neurobiol.* **54:**71–85.

Fontaine, M., Elmquist, W. F., and Miller, D. W. (1996). Use of rhodamine 123 to examine the functional activity of P-glycoprotein in primary cultured brain microvessel endothelial cell monolayers. *Life Sci.* **59:**1521–1531.

Halstead, J., Kemp, K., and Ignotz, R. A. (1995). Evidence for involvement of phosphatidylcholine-phospholipase C and protein kinase C in transforming growth factor-β signaling. *J. Biol. Chem.* **270:**13600–13603.

Hartsough, M. T., and Mulder, K. M. (1995). Transforming growth factor β activation of $p44^{mapk}$ in proliferating cultures of epithelial cells. *J. Biol. Chem.* **270:**7117–24.

Orlidge, A., and D'Amore, P. A. (1987). Inhibition of capillary endothelial cell growth by pericytes and smooth muscle cells. *J. Cell Biol.* **105:**1455–1462.

Ramsauer, M., Krause, D., and Dermietzel, R. (2002). Angiogenesis of the blood-brain barrier in vitro and the function of cerebral pericytes. *FASEB J.* **16:**1274–1276.

Raub, T. J. (1996). Signal transduction and glial cell modulation of cultured brain microvessel endothelial cell tight junctions. *Am. J. Physiol.* **271:**C495–C503.

Rubin, L. L., and Staddon, J. M. (1999). The cell biology of the blood–brain barrier. *Annu. Rev. Neurosci.* **22:**11–28.

Sato, Y., and Rifkin, D. B. (1989). Inhibition of endothelial cell movement by pericytes and smooth muscle cells: activation of a latent transforming growth factor-β1-like molecular by plasmin during co-culture. *J. Cell Biol.* **109:**309–315.

Tatsuta, T., Naito, M., Mikami, K., and Tsuruo, T. (1994). Enhanced expression by the brain matrix of P-glycoprotein in brain capillary endothelial cells. *Cell Growth Differ.* **5:**1145–1152.

Tatsuta, T., Naito, M., Oh-hara, T., Sugawara, I., and Tsuruo, T. (1992). Functional involvement of P-glycoprotein in blood-brain barrier. *J. Biol. Chem.* **267:**20383–20391.

Utsunomiya, Y., Hasegawa, H., Yanagisawa, K., and Fujita, S. (1997). Enhancement of *mdrl* gene expression by transforming growth factor-β1 in the new adriamycin-resistant human leukemia cell line ME-F_2/ADM. *Leukemia* **11:**894–895.

Wang, W., Merrill, M. J., and Borchardt, R. T. (1996). Vascular endothelial growth factor affects permeability of brain microvessel endothelial cells in vitro. *Am. J. Physiol.* **271:**C1973–C1980.

Wrana, J. L., Attisano, L., Wieser, R., Ventura, F., and Massagué, J. (1994). Mechanism of activation of the TGF-β receptor. *Nature* **370:**341–347.

プリオン蛋白高次構造を標的としたプリオン病の分子治療

Drug therapy in prion diseases

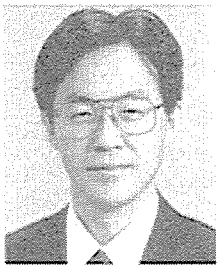

山田正仁
Masahito YAMADA
金沢大学大学院医学系研究科脳病態医学講座脳老化・神経病態学(神経内科学)

◎プリオン病は致死的な伝播性の脳疾患であり，現時点では確立した有効な治療法はない．その感染因子プリオンの主要構成成分であるプリオン蛋白(PrP)は宿主の染色体遺伝子によってコードされており，おもに中枢神経系で，少量ではリンパ系組織などに発現している．プリオン病の発症過程において，宿主の正常型のPrP(PrP^C)がプロテアーゼ抵抗性で感染型のPrP(PrP^{Sc})に高次構造(コンフォメーション)を転換することが，病態の中心をなすことが知られている．このPrPの高次構造転換過程をターゲットとして，プリオン病の予防・治療薬開発が行われている．*In vitro* の無細胞系でのPrPの転換実験，プリオン持続感染細胞を用いた実験，プリオン病動物モデルを用いた実験などの研究成果により，プリオン病の予防・治療薬候補として報告されている化合物を紹介し，そのなかでもとくに免疫学的手法による新しい治療法に焦点を当てて概説した．

Key word：プリオン病，プリオン蛋白，正常型，感染型，高次構造(コンフォメーション)

プリオン病とは

Creutzfeldt-Jakob病(CJD)などの一群の疾患は，脳組織を動物に接種すると長い潜伏期間の後に伝播されること，しばしば脳に特徴的な海綿状変化を生じることから，従来，遅発性ウイルス感染症や伝染性海綿状脳症と呼称されてきた．しかし，その感染因子として通常のウイルスとは異なるプリオンが提唱され，現在これらはプリオン病と総称されている．プリオン病はヒト以外のさまざまな動物にもみられ，ヒツジのスクレイピー，ウシのウシ海綿状脳症(BSE；狂牛病)，シカ類の慢性消耗性疾患(CWD)などが知られている(表1)．

プリオン病は種を越えて感染・伝播する人畜共通感染症である．近年，ウシのBSEに関連する変異型とよばれる新しいタイプのCJD(変異型CJD)(variant CJD：vCJD)がイギリスを中心に発生し，最近わが国でもBSEのウシが認定され，大きな問題となっている．また，ヒト屍体由来の硬膜移植後のCJDがわが国で多数発症し，これも社会問題化している．

ヒトのプリオン病はその病因から，①何の発病の背景も見出されない特発性(孤発性CJD)，②感染性，③遺伝性に大別される(表1)．

発生頻度は人口100人当り1年間にほぼ1人とされる．わが国においては，特発性の孤発性CJDが79%，プリオン蛋白遺伝子変異に伴う遺伝性プリオン病が12%，感染性プリオン病が9%を占め，感染性プリオン病はすべて硬膜移植後のCJDであった[1]．

プリオンの基本概念と疾患伝播のメカニズム

プリオン(prion)は“蛋白性の感染粒子(proteinaceous infectious particle)”を意味し，Prusinerによってスクレイピー感染脳から界面活性剤およびプロテアーゼ処理に抵抗性の感染性の強い分画に見出され，命名された[2]．プリオンの主要構成成分であるプリオン蛋白(PrP)は宿主の染色体遺伝子(PrP遺伝子)によってコードされており，おもに中枢神経系で，少量ではリンパ系組織などに発現している．その産物である正常のPrPはプロテアーゼ感受性で，感染性のない蛋白である(正常

表 1　プリオン病の分類

疾　患	宿　主
A. 動物のプリオン病	
スクレイピー(scrapie)	ヒツジ
ウシ海綿状脳症(狂牛病；bovine spongiform encephalopathy：BSE)	ウシ
ネコ海綿状脳症(feline spongiform encephalopathy：FSE)	ネコ
伝染性ミンク脳症(transmissible mink encephalopathy：TME)	ミンク
慢性消耗性疾患(chronic wasting disease：CWD)	ミュールジカ，ヘラジカ
外来有蹄類脳症(exotic ungulate encephalopathy)	ニヤラ(アフリカ産レイヨウ) クーズー(アフリカ産カモシカ)
B. ヒトのプリオン病	
特発性　孤発性(Creutzfeldt-Jakob 病：CJD)	ヒト
感染性　クールー(Kuru)	ヒト
医原性 CJD(下垂体製剤，硬膜移植後，角膜移植後など)	ヒト
変異型 CJD(variant CJD)	ヒト
遺伝性　Gerstmann-Sträussler-Scheinker 病(GSS)	ヒト
家族性 CJD	ヒト
致死性家族性不眠症(fatal familial insomnia：FFI)	ヒト

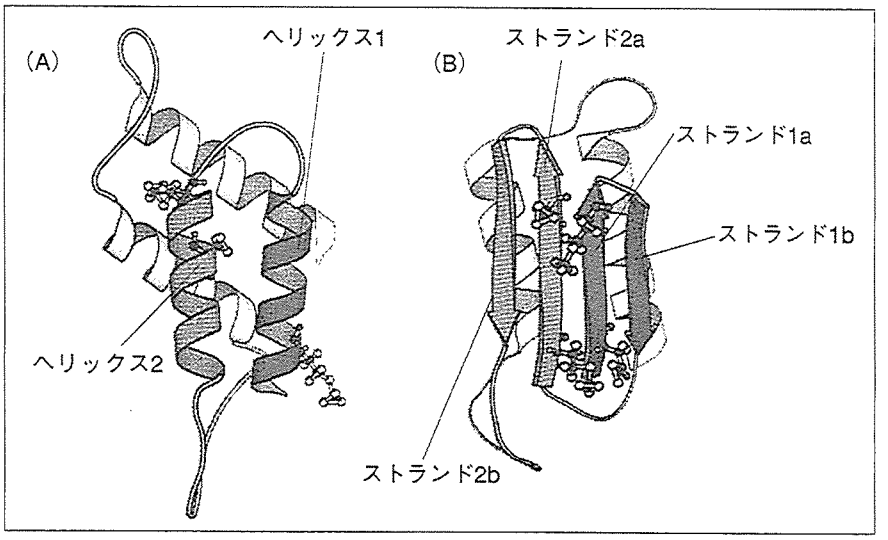

図 1　PrP^C(A)および PrP^{Sc}(B)の三次構造モデル(文献[2]より改変)
PrP^Cのヘリックス 1 を赤色で，ヘリックス 2 を緑色で示す(A)．PrP^{Sc}に転換するときにヘリックス 1 および 2 はβシート構造に転換し，PrP^{Sc}は 4 つのストランド(ヘリックス 1 由来のストランド 1a および 1b，ヘリックス 2 由来のストランド 2a および 2b)からなるβシート構造と 2 つのαヘリックス構造を含む．種間の伝播におけるバリアー(species barrier)に関係する 4 アミノ酸残基が分子模型として図示されているが(A，B)，それらはβシート構造の表面に位置し，PrP^{Sc}と PrP^Cの相互作用に関連しているらしい．

型 PrP：PrP^C)．一方，感染性の PrP は感染型 PrP (PrP^{Sc})とよばれ，プロテアーゼ抵抗性のコアを有し，PrP^Cが翻訳後にコンフォメーションの変化を起こし，βシート構造に富むようになることでつくり出される(図 1)[2]．PrP^Cから PrP^{Sc}へのコンフォメーションの変化に伴う PrP^{Sc}の蓄積，あるいは正常の PrP^C機能の消失によりニューロンやシナプスの障害が生じると考えられている．この感染因子プリオンによる共通のメカニズムによって，CJD，スクレイピーをはじめとする一群の疾患が発症するという仮説(プリオン仮説)は，現在広く受け入れられている．PrP^Cが発現していない宿主にはプリオン病は感染しない．

感染因子プリオンは種を越えて伝播し，プリオン病を引き起こす．一般に，近縁の種の間では伝播を起こしやすく，遠い種では伝播が起こりにく

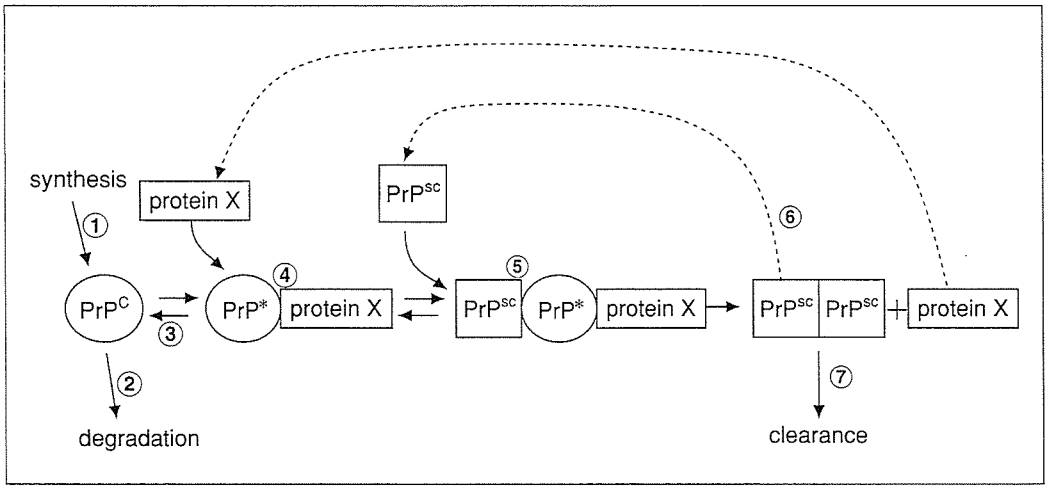

図 2　PrP^Cから PrP^{Sc}への転換(template-assisted PrP^{Sc} formation)を示す模式図(文献[2]より改変)

細胞内で産生された PrP^Cは PrP*(PrP 転換の際の中間体)として, protein X(PrP 転換に寄与する要素として想定されている因子)と結合する. つぎに, PrP^{Sc}が PrP*/protein X 複合体に結合する. PrP*が PrP^{Sc}に変換するとき, protein X はリリースされる. この転換過程を阻止する戦略として, ①PrP^C産生の阻害, ②PrP^C分解経路の促進, ③PrP^Cの安定化による PrP*への転換阻止, ④protein X の結合阻害, ⑤PrP^C/PrP*と PrP^{Sc}の相互作用阻害, ⑥PrP^{Sc}を隔離することにより PrP 転換のための鋳型(template)として利用できないようにする, ⑦PrP^{Sc}のクリアランスを促進することなどが考えられている.

いことが知られている(species barrier). 種を越えた伝播の起こりやすさには, PrP 自体の種差, PrP^Cから PrP^{Sc}への転化に関与する分子シャペロン(protein X)の種差などが関係しているものと考えられている.

また, 伝播の経路が重要であり, 感染脳のホモジネートを実験動物の脳内に直接接種すればもっとも伝播が成立しやすい. ウシの BSE がヒトへ感染し vCJD を発症することが問題となっているが, そうした場合, 経口的に摂取された BSE 因子が消化管から脳に到達し, vCJD を発症させる伝播経路が問題になる. vCJD では PrP を発現しているリンパ系組織(消化管粘膜リンパ装置, リンパ節, 扁桃, 脾など)で PrP^{Sc}が蓄積しており, そこから末梢神経系を通じて中枢神経系に伝播していく可能性が指摘されている. また, 末梢ルートで投与された下垂体製剤(成長ホルモン, ゴナドトロピン)や, プリオンの腹腔内投与による動物伝播実験などでも末梢でいったん感染が成立し(末梢における PrP^{Sc}の複製), その後中枢神経系に伝播していく(中枢神経系への PrP^{Sc}の侵入).

また, 同じ種においても異なったプリオン病の表現型(潜伏期間や臨床・病理像)をもたらす, 多様なプリオンの"株(strain)"が存在し, これらは PrP^{Sc}の異なったコンフォメーションを反映している可能性が指摘されている.

プリオン蛋白の高次構造変換のメカニズムとそれに基づく治療戦略

PrP^Cから PrP^{Sc}への高次構造変換を抑えることがプリオン病の予防・治療薬開発の基本戦略となっている. しかし, この高次構造変換の正確なメカニズムはいまだ解明されていない.

PrP^Cから PrP^{Sc}への高次構造変換について現在考えられているのは, おもに 2 つのモデルである. ひとつは PrP^{Sc}がシード(seed)として働き, それを核として PrP^Cが立体構造を変えてあらたな PrP^{Sc}としてつぎつぎに付加され, PrP^{Sc}の重合体ができていくという重合モデル, もうひとつは PrP^{Sc}が PrP^Cと複合体をつくり(PrP^C-PrP^{Sc} heterodimer complex), PrP^Cを PrP^{Sc}に転換させていくというヘテロダイマーモデルである(図 2)[2]. 後者のモデルに基づいて, そのさまざまな段階に修飾を加えることによって疾患の発症を予防・治療しようとする試みがなされている(図 2). それらには PrP^C合成の阻害(図 2-①)[3]から生成された PrP^{Sc}のクリ